Available online at www.sciencedirect.com

SciVerse ScienceDirect

journal homepage: www.elsevier.com/locate/he

Short Communication

Carbon supported MnO_x–Co_3O_4 as cathode catalyst for oxygen reduction reaction in alkaline media

Ying Wang [a,b], Xiangyuan Ma [a], Liujin Lu [a], Yude He [a], Xiujuan Qi [a], Youquan Deng [a,*]

[a] Centre for Green Chemistry and Catalysis, Lanzhou Institute of Chemical Physics, Chinese Academy of Sciences, Lanzhou 730000, China

[b] University of Chinese Academy of Sciences, Beijing 100039, China

ARTICLE INFO

Article history:
Received 11 June 2013
Received in revised form
6 August 2013
Accepted 8 August 2013
Available online 5 September 2013

Keywords:
Manganese oxides
Cobalt oxides
Oxygen reduction reaction
Alkaline media

ABSTRACT

The electroreduction of oxygen of MnO_x–Co_3O_4/C was firstly studied in alkaline media. The MnO_x–Co_3O_4/C showed better electrocatalytic activity towards ORR than MnO_x/C and Co_3O_4/C. Compared to Pt/C, MnO_x–Co_3O_4/C showed better methanol tolerance and durability in alkaline solution. Thus, the MnO_x–Co_3O_4/C catalyst had potential for applications in metal–air batteries and alkaline fuel cells.

1. Introduction

Oxygen reduction reaction (ORR) is of great importance to metal–air batteries and fuel cells. Pt-based materials have been recognized as the most efficient catalysts for ORR [1], but they are seriously suffered from the high cost and shortage resource. Recently, some non-Pt electrocatalysts have shown their significant activities including Pd [2], Ag [3], N-doped materials [4], metal chalcogenides [5], as well as transition metal oxides [6–8]. Among these substitutes, transition metal oxides have attracted much attention because of their low cost, high activity and environmental friendship.

Manganese oxides as one kind of the transition metal oxides have been applied as promising catalysts for ORR. Their activity depends on chemical composition, structure, morphology, and preparation method [9]. Sun et al. [10] synthesized the carbon-supported $Ni(OH)_2$–MnO_x/C by reducing the amorphous MnO_2/C in the presence of Ni^{2+} with $NaBH_4$ and found its activity and stability were improved. Cheng et al. [11] found a facile strategy for improving the activity of MnO_2 by generating native oxygen deficiency without introducing foreign components, and this oxide showed more positive potential and lower peroxide yield.

Cobalt oxides (Co_3O_4) as spinel structure material have been investigated as non-precious ORR catalysts and applied in metal–air batteries. The reported Co_3O_4/N-doped graphene material [7] exhibited comparable activity to commercial Pt/C but far exceeding Pt/C in stability. In order to further improve

* *Corresponding author*. Tel.: +86 931 4968116.
E-mail address: ydeng@licp.cas.cn (Y. Deng).

0360-3199/$ – see front matter
http://dx.doi.org/10.1016/j.ijhydene.2013.08.048

the activity, some hybridized oxides were prepared. Ye et al. [12] developed hierarchical Fe_3O_4–Co_3O_4 yolk-shell nanostructures by a facile template-free rout and found it showed higher activity than Fe_3O_4 and Co_3O_4.

Currently, hybrid MnO_2/Co_3O_4 nanomaterial as bifunctional oxygen cathode catalyst was reported [13] and exhibited enhanced activity for ORR and oxygen evolution reaction. However, to our knowledge, no studies have reported the ORR activity and methanol tolerance of MnO_x–Co_3O_4/C in alkaline media. In this work, we investigated the ORR catalytic activity for MnO_x–Co_3O_4/C in alkaline media. This catalyst showed higher activity than MnO_x/C and Co_3O_4/C and better methanol tolerance than Pt/C in alkaline solution.

2. Experimental

The Co_3O_4/C (Vulcan XC-72R, Cobot Corp.) was prepared as described by Liang et al. [7]. Briefly, a mixture was prepared by adding 5.7 mL of 0.2 M $Co(OAc)_2$ aqueous solution to 50 mL carbon black ethanol suspension (0.01 g/mL), followed by the addition of 1.5 mL NH_4OH (30% solution). After that, the mixture was stirred for 10 h at 80 °C, and then transferred to autoclave for hydrothermal reaction at 150 °C for 3 h. The prepared Co_3O_4/C was washed with ethanol and water, and dried in air at 80 °C. For MnO_x–Co_3O_4/C, 0.1 g Co_3O_4/C was added into 20 mL distilled water with continuous stirring. Then $KMnO_4$ solution with calculated concentration of 0.2 wt.% was slowly added into the suspension prepared before. After the mixture was kept at 70 °C for 1 h, the suspension was filtered, washed, and dried at 80 °C overnight. The MnO_x loading was calculated as 10 wt.%. The 10 wt.% MnO_x/C catalyst was prepared through the same steps as MnO_x–Co_3O_4/C. The 20 wt.% Pt/C catalyst was prepared by ethylene glycol (EG) method [14].

X-ray diffraction (XRD) measurements were performed using Siemens D/max-RB powder X-ray diffractometer with Cu Kα1 radiation (40 mA, 40 kV). The X-ray photoelectron spectroscopy (XPS) was recorded by VG ESCALAB 210 instrument using a Mg Kα radiation (1253.6 eV). The actual loading were analyzed by Atomic Absorption Spectrometer (AAS, ContrAA700). Digestion involved heating sample in $HClO_4$–HNO_3 mixture to fuming and then taking it to dryness. The residue was dissolved in aqua regia. After boiled for 20 min, the solution was transferred into 50 mL volumetric flask. The loadings of MnO_x, Co_3O_4 and Pt were about 9.8 wt.%, 3.5 wt.% and 19.5 wt.%, respectively. The standard deviation obtained from analysis was shown in Table 1.

Rotating disk electrode (RDE) measurements (ATA-1B, Jiangfen, 3 mm diameter) were performed on electrochemical workstation system (CHI 660A) with a conventional three electrode cell. A Pt wire and Hg/HgO electrode (0.93 vs RHE) were used as counter electrode and reference electrode, respectively. Typically, 5 mg catalyst was ultrasonically suspended in 0.5 mL ethanol and 25 μL 5 wt.% Nafion solution for about 30 min, then 3 μL slurry was coated on the surface of GC electrode. The catalyst loading on the electrode was calculated as 402 μg cm^{-2}. The onset potential is determined by the point of intersection of two tangent lines, one drawn parallel to the baseline (*i.e.*, from 1.0 to 0.9 V), and the other parallel to the linearly increasing portion of the oxygen–reduction curve [15]. Kinetic currents were calculated by $i_k = i/(1 - i/i_d)$, where i is the measured current and i_d is the diffusion limited current at 0.43 V. The ORR polarization curves were corrected by subtracting background current measured under N_2 atmosphere. The electrochemical surface areas (ESA) were calculated by analyzing the double-layer capacitance under potential steps method using double-layer capacitance of pure mercury 20 μF cm^{-2}, and the change of the potential was 10 mV.

The performance of zinc air battery was tested using a LAND battery testing system (Wuhan Jinnuo Company). A polished zinc plate and a piece of catalyst coated gas diffusion layer (1 cm × 1 cm) were used as anode and cathode. The catalyst loading was 4 mg cm^{-2} and the electrolyte was 6 M KOH solution.

Table 1 – Standard deviation obtained from AAS and comparison of onset potential (E_{onset}) and half-wave potential ($E_{1/2}$) for different catalysts.

Samples	Standard deviation (wt.%)	E_{onset} (mV)	$E_{1/2}$ (mV)
Co_3O_4/C	0.11	834	788
MnO_x/C	0.28	850	791
MnO_x–Co_3O_4/C	0.31[a] 0.09[b]	874	814
Pt/C	0.21	911	870

a Standard deviation for MnO_x.
b Standard deviation for Co_3O_4.

3. Results and discussions

XRD patterns of samples are shown in Fig. 1a. All samples showed a broad peak located at about 25.0°, which is attributed to the graphite (002) of carbon [16]. For Co_3O_4/C, the peaks at about 31.3°, 36.8°, 59.4° and 65.2° were attributed to (220), (311), (511) and (440) planes, respectively, which means the formation of Co_3O_4. For MnO_x/C, two broad peaks at 36.8° and 66.2° assigned to (006) and (119) planes of MnO_2 (PDF#18-0802), respectively, including its amorphous structure. Compared to Co_3O_4/C, the two diffraction peaks of MnO_x–Co_3O_4/C at 36.8° and 65.6° had the same intensity, but slightly broadening, which can be due to the amorphous structure of MnO_x. These two peaks should be attributed to the overlap of diffraction peaks of Co_3O_4 and MnO_x. Fig. 1b–d shows TEM images of catalysts. The MnO_x nanosheets with 20–80 nm in length presented in MnO_x/C and MnO_x–Co_3O_4/C. For MnO_x–Co_3O_4/C, MnO_x nanosheets were not well uniformly distributed with some agglomeration in some locations. Compared to ref. [13], some Co_3O_4 nanoparticles were dispersed around MnO_x nanosheets and they were individually located on the carbon, which may increase the active sites.

Fig. 1e shows the XPS spectra of Co2p. Two doublet peaks with binding energy position at 795.9 eV ($Co2p_{1/2}$) and 780.7 eV ($Co2p_{3/2}$) were observed, indicating the presence of Co^{2+}/Co^{3+} species [17]. Weak 2p satellite features are found with binding energies at 789.3 and 804.7 eV. It has been reported that the weak satellite peaks are characteristic of spinel structures in

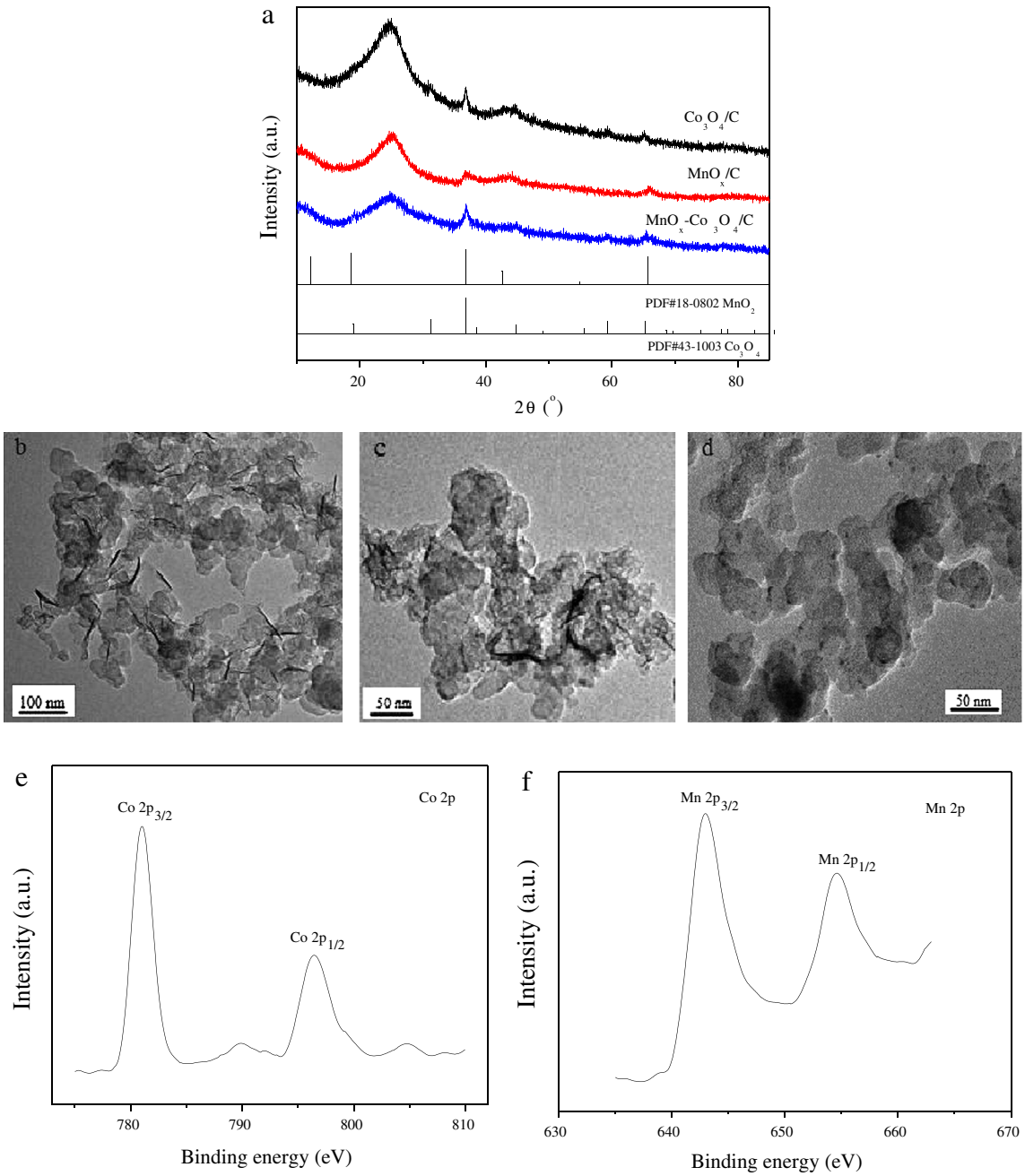

Fig. 1 – (a) XRD patterns of Co_3O_4/C, MnO_x/C and MnO_x–Co_3O_4/C samples. (b), (c) and (d) TEM images of MnO_x/C, MnO_x–Co_3O_4/C and Co_3O_4/C. (e) and (f) Co 2p and Mn 2p XPS spectra of MnO_x–Co_3O_4/C.

which 3+ cations occupy octahedral lattice sites, and 2+ cations are in tetrahedral sites [18]. The XPS spectra of $Mn2p_{3/2}$ and $Mn2p_{1/2}$ is shown in Fig. 1f. Two strong peaks centered at 642.5 and 654.1 eV were found with a spin-energy separation 11.6 eV, which confirmed the presence of Mn (IV) state. The Mn/Co atomic ratio was 3.0, which was higher than the bulk atomic ratio (2.4). It indicates the enrichment of MnO_x at the surface of catalyst.

The cyclic voltammogram (CV) curves for samples in N_2- and O_2-saturated 1 M KOH solution are shown Fig. 2a. For Co_3O_4/C, the anodic and corresponding cathodic peaks between 0.93 and 1.23 V can be attributed to the redox transition of Co^{2+}/Co^{3+}. May be the redox transition of Co^{3+}/Co^{4+} was at higher potentials (>1.43 V), so the peaks of Co^{3+}/Co^{4+} were not observed. The addition of MnO_x resulted in the peak overlap between Co_3O_4 and MnO_x, and the CV curve for MnO_x–Co_3O_4/C was similar to that of MnO_x/C. During the cathodic scanning (inset to Fig. 2a), there was a reduction peak located at 0.83 V. According to previously reported XANES results [19], the peak represented the conversion of Mn (IV) to Mn (III). When further lowering the potential to 0.63 V, the peak with higher current was observed. It shows the transition of Mn (III) to Mn (II) and the formation of intermediate product Mn_3O_4. In the positive direction, the peaks located at 0.71 and 0.90 V were attributed to

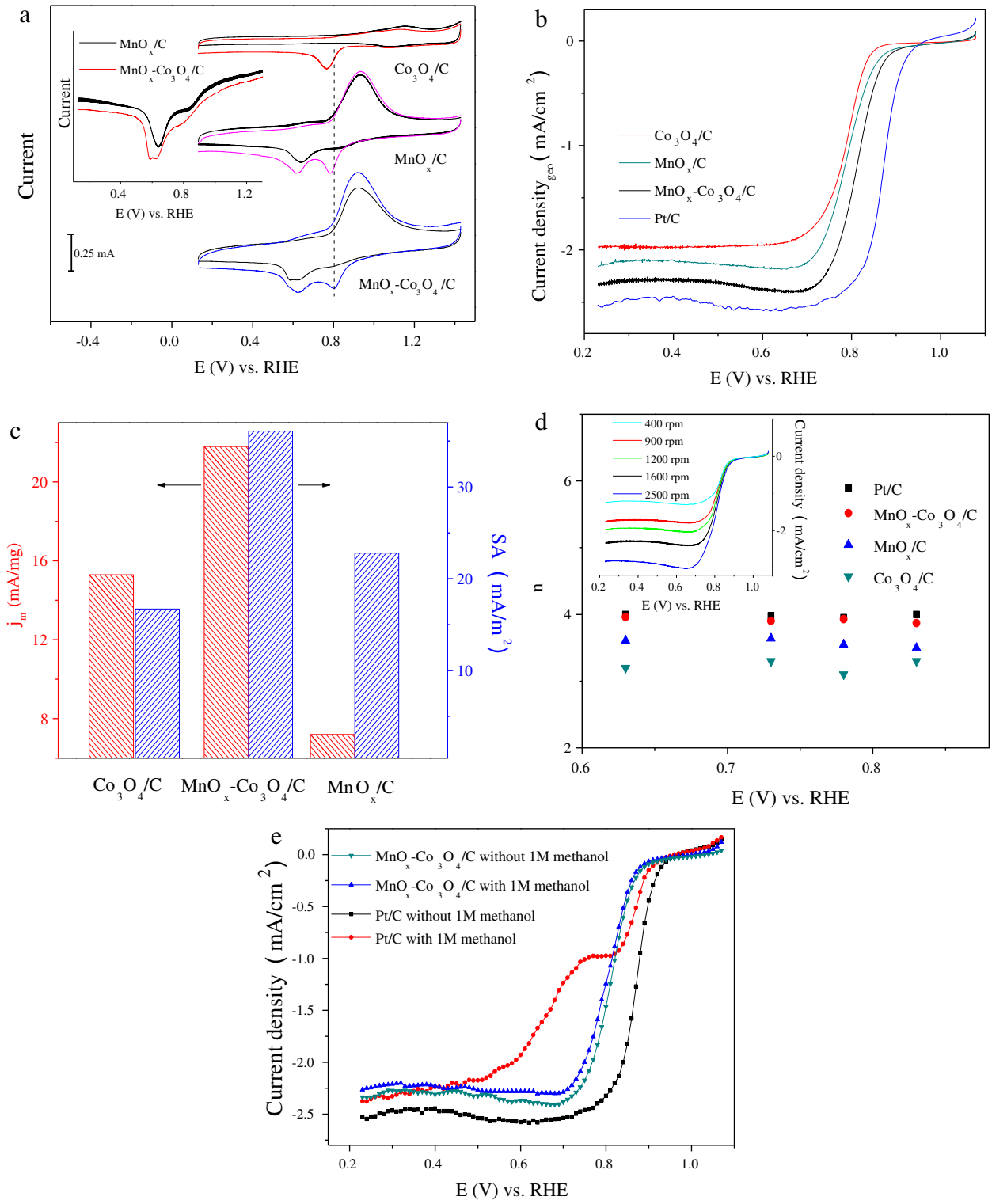

Fig. 2 – (a) CV curves of Co_3O_4/C, MnO_x/C and MnO_x–Co_3O_4/C samples in N_2-(black curve) and O_2-saturated 1 M KOH solution at a scan rate of 100 mV s^{-1}. The inset presents the cathodic scanning curves of MnO_x/C and MnO_x–Co_3O_4/C in N_2-saturated solution. (b) The polarization curves for ORR on Co_3O_4–C, MnO_x/C, MnO_x–Co_3O_4/C and Pt/C in O_2-saturated 1 M KOH solution at 1600 rpm. (c) Comparison of specific activity and mass activity at 0.83 V. (d) The number (*n*) of electrons transferred. The inset shows polarization curves for ORR on MnO_x–Co_3O_4/C in O_2-saturated. (e) Linear potential scan curves in 1 M KOH solution containing 1 M methanol.

the oxidation of Mn (II) to Mn (III). When the potential was scanned positively to 1.33 V, no obvious peaks appeared. The slight conversion of Mn (III) to Mn (IV) may be concealed in the increasing background current [10]. In O_2-saturated solution, the ORR peak at about 0.73 V can be observed. For MnO_x–Co_3O_4/C, it appeared at more positive potential compared to Co_3O_4/C and MnO_x/C, indicating that MnO_x–Co_3O_4/C had better activity for ORR.

To further investigate the ORR activity, the polarization curves of catalysts in O_2-saturated solution were measured (Fig. 2b). As can be seen in Table 1, though the activity of MnO_x–Co_3O_4/C was not as high as Pt/C, the onset and half-wave potentials of MnO_x–Co_3O_4/C were higher than those of Co_3O_4/C and MnO_x/C, indicating the integration of MnO_x with Co_3O_4 improves ORR catalytic activity. According to the report from Tseung et al. [20], cobalt oxide is an efficient synergistic component for other ORR catalysts due to the capability of catalyzing the disproportionation reaction of intermediater in oxygen electroreduction. It has been reported that ORR on MnO_x is achieved through 2 × 2e pathway [21]. Hence, Co_3O_4 can help to promote the reduction of HO_2^- to OH^- and enhance the oxygen reduction reaction. Meanwhile, Co_3O_4 has high affinity towards oxygen, which can favor the chemisorptions of oxygen molecules on catalyst surface [17] and facilitate oxygen transport. Co_3O_4 can reduce the O_2 as well as MnO_x, so a collaborative effect between MnO_x and Co_3O_4 leads to the enhanced catalytic performance. In order to characterize the intrinsic catalytic activity, the specific activity (SA) and mass activity (j_m) normalized by the metal oxide mass at 0.83 V were compared (Fig. 2c). The ESA were calculated by analyzing the double-layer capacitance, and the j_m were calculated by $j_m = i_k/L_{cat}$, where L_{cat} is the metal oxide mass. The ESA values were about 11.5, 18.1 and 24.2 cm^2 for Co_3O_4–C, MnO_x/C and MnO_x–Co_3O_4/C, respectively. As can be seen, The SA for MnO_x–Co_3O_4/C was higher than those of Co_3O_4–C and MnO_x/C, and the j_m of MnO_x–Co_3O_4/C was 21.8 mA/mg, which was 1.4 times higher than that of Co_3O_4/C, even higher than that of the reported Ag/Co_3O_4–C [22]. It suggests that the MnO_x–Co_3O_4/C as a more economic ORR catalyst can be applied in metal–air batteries and alkaline fuel cells.

The number (n) of electrons transferred obtained by Koutecky–Levich plots are shown in Fig. 2d, and the inset displays the polarization curves of MnO_x–Co_3O_4/C under different rotating rates. For Pt/C, the n was close to four, which is consistent with the results reported [23,24]. The n value for MnO_x–Co_3O_4/C was about 3.9, indicating that ORR on it proceeds by a quasi-4e pathway. The fact that more peroxide produced on Co_3O_4/C is probably due to the low Co_3O_4 loading on carbon support, where the ORR occurs mainly through 2-electron pathway [25].

The methanol tolerance towards ORR over the MnO_x–Co_3O_4/C and Pt/C was evaluated in O_2-saturated 1 M KOH + 1 M CH_3OH solution (Fig. 2e). A shoulder at 0.73 V can be observed for Pt/C and the current density decreased by 54% at 0.73 V, indicating the occurrence of methanol oxidation reaction [26], whereas the presence of methanol did not change the shape of polarization curve for MnO_x–Co_3O_4/C, and the current density retained about 91%. The results shows that the MnO_x–Co_3O_4/C has higher selectivity for ORR in methanol-containing alkaline solution than Pt/C, although MnO_x–Co_3O_4/C does not have a complete methanol tolerance.

The durability of MnO_x–Co_3O_4/C was evaluated at 0.73 V (Fig. 3a). The ORR currents for both MnO_x–Co_3O_4/C and Pt/C decreased with time, but MnO_x–Co_3O_4/C showed a slower decrease than Pt/C, demonstrating a good catalytic stability of MnO_x–Co_3O_4/C over Pt/C in alkaline solution. The MnO_x–Co_3O_4/C as cathode electrode in a single zinc air battery was evaluated at room temperature (Fig. 3b). The open circuit voltage of the single cell was around 1.39 V and maximum power density was 97 mW cm^{-2} at 0.97 V, which was much higher than MnO_2/Co_3O_4 [13].

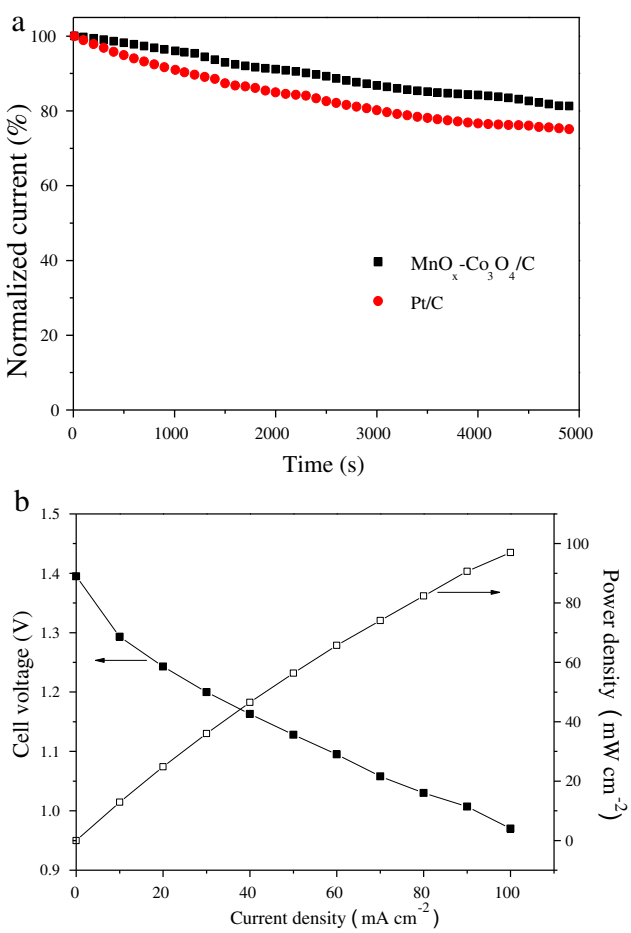

Fig. 3 – (a) Chronoamperometric responses of MnO_x–Co_3O_4/C and Pt/C at 0.73 V. (b) Single cell performance of zinc air battery using MnO_x–Co_3O_4/C electrocatalyst in 6 M KOH.

4. Conclusion

The hybrid catalyst MnO_x–Co_3O_4/C was found to have better activity for ORR than MnO_x/C and Co_3O_4/C in alkaline solution. Electrochemical characterizations demonstrated that the ORR on this catalyst proceeded by a 4-electron transfer pathway. MnO_x–Co_3O_4/C showed better durability and methanol tolerance than Pt/C. Using MnO_x–Co_3O_4/C as cathode electrode, zinc air battery had the power density of 97 mW cm^{-2}.

Acknowledgments

This work was supported by the National Natural Science Foundation of China (No. 21373247) and the Science and Technology Pillar Program of Gansu Province, PR China (1104GKCA041).

REFERENCES

[1] Wang D, Xin HL, Hovden R, Wang H, Yu Y, Muller DA, et al. Structurally ordered intermetallic platinum-cobalt core-shell nanoparticles with enhanced activity and stability as oxygen reduction electrocatalysts. Nat Mater 2013;12:81–7.
[2] Takenaka S, Susuki N, Miyamoto H, Tanabe E, Matsune H, Kishida M. Highly durable carbon nanotube-supported Pd catalysts covered with silica layers for the oxygen reduction reaction. J Catal 2011;279:381–8.
[3] Lee CL, Tsai YL, Huang CH, Huang KL. Performance of silver nanocubes based on electrochemical surface area for catalyzing oxygen reduction reaction. Electrochem Commun 2013;29:37–40.
[4] Nagaiah TC, Kundu S, Bron M, Muhler M, Schuhmann W. Nitrogen-doped carbon nanotubes as a cathode catalyst for the oxygen reduction reaction in alkaline medium. Electrochem Commun 2010;12:338–41.
[5] Feng Y, Alonso-Vante N. Carbon-supported cubic $CoSe_2$ catalysts for oxygen reduction reaction in alkaline medium. Electrochim Acta 2012;72:129–33.
[6] Wu ZS, Yang S, Sun Y, Parvez K, Feng X, Müllen K. 3D nitrogen-doped graphene aerogel-supported Fe_3O_4 nanoparticles as efficient electrocatalysts for the oxygen reduction reaction. J Am Chem Soc 2012;134:9082–5.
[7] Liang Y, Li Y, Wang H, Zhou J, Wang J, Regier T, et al. Co_3O_4 nanocrystals on graphene as a synergistic catalyst for oxygen reduction reaction. Nat Mater 2011;10:780–6.
[8] Roche I, Chaînet E, Chatenet M, Vondrák J. Carbon-supported manganese oxide nanoparticles as electrocatalysts for the oxygen reduction reaction (ORR) in alkaline medium: physical characterizations and ORR mechanism. J Phys Chem C 2007;111:1434–43.
[9] Cheng F, Shen J, Ji W, Tao Z, Chen J. MnO_2-based nanostructures as catalysts for electrochemical oxygen reduction in alkaline media. Chem Mater 2010;22:898–905.
[10] Wu Q, Jiang L, Tang Q, Liu J, Wang S, Sun G. Activity and stability of the $Ni(OH)_2$-MnO_x/C composite for oxygen reduction reaction in alkaline solution. Electrochim Acta 2013;91:314–22.
[11] Cheng F, Zhang T, Zhang Y, Du J, Han X, Chen J. Enhancing electrocatalytic oxygen reduction on MnO_2 with vacancies. Angew Chem Int Ed 2013;52:2474–7.
[12] Ye Y, Kuai L, Geng B. A template-free route to Fe_3O_4-Co_3O_4 yolk-shell nanostructure as a noble-metal free electrocatalyst for ORR in alkaline media. J Mater Chem 2012;22:19132–8.
[13] Du G, Liu X, Zong Y, Andy Hor TS, Yu A, Liu Z. Co_3O_4 nanoparticle-modified MnO_2 nanotube bifunctional oxygen cathode catalysts for rechargeable zinc-air batteries. Nanoscale 2013;5:4657–61.
[14] Li W, Zhou W, Li H, Zhou Z, Zhou B, Sun G, et al. Nano-stuctured Pt-Fe/C as cathode catalyst in direct methanol fuel cell. Electrochim Acta 2004;49:1045–55.
[15] Shi Y, Yang R, Yue PK. Easy decoration of carbon nanotubes with well dispersed gold nanoparticles and the use of the material as an electrocatalyst. Carbon 2009;47:1146–51.
[16] Yang Z, Zhou X, Nie H, Yao Z, Huang S. Facile construction of manganese oxide doped carbon nanotube catalysts with high activity for oxygen reduction reaction and investigations into the origin of their activity enhancement. ACS Appl Mater Inter 2011;3:2601–6.
[17] Xu J, Gao P, Zhao TS. Non-precious Co_3O_4 nano-rod electrocatalyst for oxygen reduction reaction in anion-exchange membrane fuel cells. Energy Environ Sci 2012;5:5333–9.
[18] Fu L, Liu Z, Liu Y, Han B, Hu P, Cao L, et al. Beaded cobalt oxide nanoparticles along carbon nanotubes: towards more highly integrated electronic devices. Adv Mater 2005;17:217–21.
[19] Lima FHB, Calegaro ML, Ticianelli EA. Electrocatalytic activity of manganese oxides prepared by thermal decomposition for oxygen reduction. Electrochim Acta 2007;52:3732–8.
[20] Jiang SP, Lin ZG, Tseung ACC. Homogeneous and heterogeneous catalytic reactions in cobalt oxide/graphite air electrodes. J Electrochem Soc 1990;137:759–64.
[21] Cao YL, Yang HX, Ai XP, Xiao LF. The mechanism of oxygen reduction on MnO_2-catalyzed air cathodin alkaline solution. J Electroanal Chem 2003;557:127–34.
[22] Wang Y, Lu X, Liu Y, Deng Y. Silver supported on Co_3O_4 modified carbon as electrocatalyst for oxygen reduction reaction in alkaline media. Electrochem Commun 2013;31:108–11.
[23] Jiang L, Hsu A, Chu D, Chen R. Oxygen reduction on carbon supported Pt and PtRu catalysts in alkaline solutions. J Electroanal Chem 2009;629:87–93.
[24] Meng H, Shen PK. Novel Pt-free catalyst for oxygen electroreduction. Electrochem Commun 2006;8:588–94.
[25] Perez J, Gonzalez ER, Ticianelli EA. Oxygen electrocatalysis on thin porous coating rotating platinum electrodes. Electrochim Acta 1998;44:1329–39.
[26] Liu SH, Chen SC, Sie WH. Heat-treated platinum nanoparticles embedded in nitrogen-doped ordered mesoporous carbons: synthesis, characterization and their electrocatalytic properties toward methanol-tolerant oxygen reduction. Int J Hydrogen Energy 2011;36:15060–7.